Paez *et al*., 2004). A mutation conferring resistance to these two kinase inhibitors, T790M (exon 20), has also been found in the EGFR kinase domain and can account for about half of the cases of acquired resistance (Kobayashi *et al*., 2005). There are a number of other kinase domain mutations of EGFR that occur at lower frequencies, most often in combination with L858R (Tam *et al*., 2006). However, how these mutations might interact when present together in-*cis* is unknown.

We recently identified a novel EGFR kinase domain somatic mutation, E884K (Glu884Lys, exon 22) in a patient with stage IV non-small-cell lung cancer, in combination with the L858R mutation (L858R + E884K) (Choong *et al*., 2006). The patient initially received carboplatin/paclitaxel and erlotinib and then developed brain metastasis on maintenance erlotinib. In spite of further treatment with whole brain radiation, temozolomide and irinotecan, the patient's disease progressed to symptomatic leptomeningeal carcinomatosis, which responded to gefitinib, a year after being off an EGFR kinase inhibitor. The L858R + E884K double mutation was found both in her pretreatment diagnostic thoracic lymph node biopsy specimen as well as in the tumor cells (extracted by laser microdissection) within the cerebrospinal fluid during the course of leptomeningeal metastases (Choong *et al*., 2006). The E884K mutation represents the first mutation reported to show an apparent differential response to the two EGFR kinase inhibitors erlotinib and gefitinib, whereas L858R was known to be sensitizing to both. These findings led to our hypothesis that EGFR kinase mutations can work together to differentially alter inhibitor sensitivity and downstream signaling. Further biochemical analysis in our current study indicates that the double mutant EGFR (L858R + E884K) responds differently to gefitinib and erlotinib. We now show that E884K works in concert with L858R, and in a dominant manner, to mediate differential sensitivity to kinase inhibitors through altered phosphorylation of AKT and signal transducer and activator of transcription 3 (STAT3) and were correlated with differential cellular cytotoxicity and induction of the apoptotic marker cleaved-PARP(Asp214) by EGFR inhibitors. Using a combination of bioinformatics and structural analyses, we further characterized the role of the E884 residue in EGFR kinase function. Our results further demonstrate that the ion pair formed by residues E884 and R958 in the EGFR kinase domain is a highly conserved feature of protein kinases in the human kinome, including many 'druggable' targets such as MET. Disruption of the conserved ion pair in EGFR modulates downstream signal transduction and differentially alters kinase inhibitor sensitivity in an inhibitor-specific manner.

Results

E884K works in concert with L858R mutation to confer differential inhibitor sensitivity through inhibition of AKT and STAT3 downstream signaling

We hypothesize that EGFR kinase mutations can work together to differentially alter inhibitor sensitivity. To test this hypothesis, *EGFR* expression constructs engineered with L858R (LR) or dual mutations of L858R + E884K (LR + EK) were stably transfected into COS-7 cells. Cells were treated with increasing concentrations of either erlotinib or gefitinib in the presence of EGF stimulation (Figure 1a). Compared with L858R alone, the L858R + E884K dual mutant was less sensitive to erlotinib in the inhibition of tyrosine phosphorylation of EGFR. Conversely, E884K worked in concert with L858R in-*cis* to further enhance the sensitivity of the mutant receptor to gefitinib inhibition (Figures 1a and b). These findings correlated with the clinical course of the patient's response profile (Choong *et al*., 2006) and highlight the potential for EGFR kinase mutations to exert concerted effects in-*cis* to impact targeted inhibition.

To gain insight into the mechanism of E884K modulation of EGFR tyrosine kinase inhibitor (TKI) sensitivity, we further studied its effect on downstream AKT and STAT3 signaling pathways with TKI inhibition. The effect on the downstream signal mediators p-AKT (S473) and p-STAT3 (Y705) correlated well with the inhibition of EGFR phosphorylation (Figure 1a); E884K in-*cis* with L858R decreased erlotinib inhibition of AKT and STAT3 phosphorylation but increased inhibition by gefitinib. The differential inhibition exerted by E884K on EGFR, AKT and STAT3 signaling also corresponded to the inhibitor-induced expression pattern of the apoptotic marker, cleaved-PARP(Asp214) (Figure 1c). Similarly, there was an opposite effect of the E884K mutation over L858R in-*cis* in inducing cellular cytotoxicity by erlotinib and gefitinib (Figure 1d). Hence, E884K in-*cis* with L858R differentially altered inhibitor sensitivity when compared with L858R alone, through differential inhibition of the prosurvival AKT and STAT3 signaling pathways associated with altered induction of cleaved-PARP(Asp214).

E884K-EGFR modulates inhibitor sensitivity effects in an inhibitor-specific manner

To further examine the hypothesis that EGFR mutations exert effects in combination that are unique to a specific kinase inhibitor, we further tested the mutant EGFR expressing L858R alone or L858R + E884K in-*cis*, against several other ERBB family TKIs, including both reversible inhibitors (4557W, Lapatinib, GW583340, Tyrphostin-AG1478) and irreversible inhibitor (CL-387,785) (Figure 2 and Supplementary Figure 2). We focused on the effects of these inhibitors on the sensitivity of inhibition of the EGFR kinase phosphorylation in the mutant EGFR. As the tyrosine phosphorylation of the EGFR has been shown to correlate well with its catalytic enzymatic activity, we used the tyrosine phosphorylation of the pY1068 (GRB1-binding site) epitope of EGFR as the surrogate measurement of the extent of inhibition by the TKIs. For 4557W (reversible dual TKI of EGFR/ERBB2), the E884K mutation modulated the L858R mutation in-*cis*, again in a dominant manner, rendering the double-mutant receptor more sensitive to the dual inhibitor

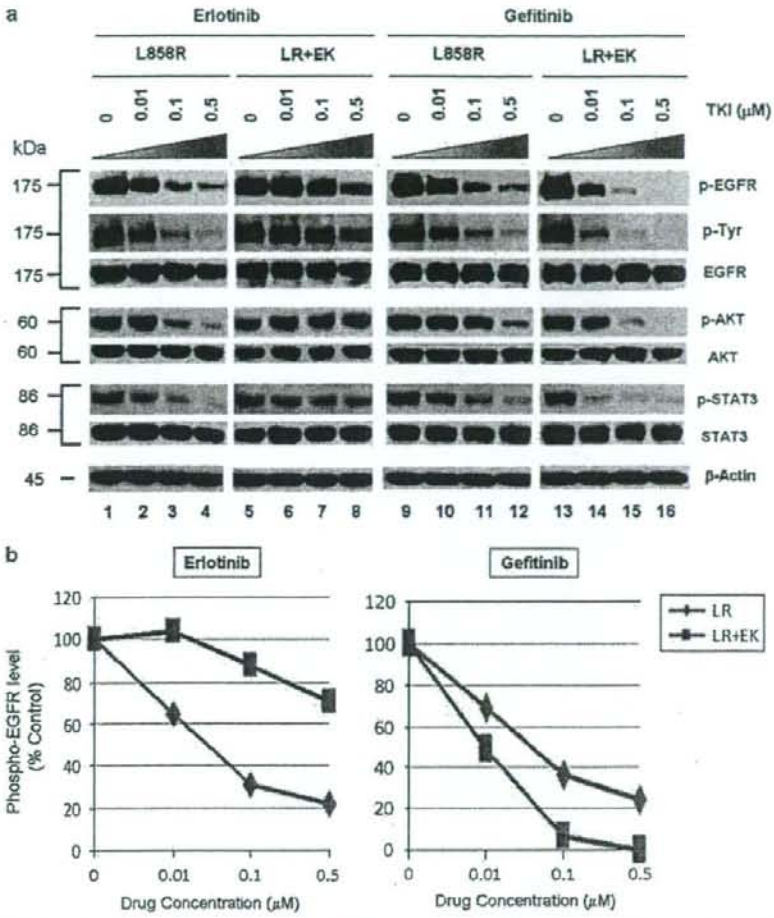

Figure 1 E884K mutation of epidermal growth factor receptor (EGFR) worked in concert with L858R to differentially alter sensitivity to EGFR kinase inhibitors erlotinib and gefitinib. (**a**) Stable COS-7 transfects expressing the L858R and double-mutant L858R + E884K variants of *EGFR* were used in the experiment. The endogenous wild-type EGFR expression of parental COS-7 cells is negligible (data not shown). Cells were cultured in 0.5% bovine serum albumin-containing serum-free media for 16 h and then incubated with increasing concentrations of either erlotinib or gefitinib in the presence of EGF (100 ng/ml). Whole-cell lysates were extracted for SDS polyacrylamide gel electrophoresis and immunoblotting using antibodies against: p-EGFR (Y1068), phosphotyrosine (p-Tyr), EGFR, p-AKT (S473), AKT, p-STAT3 (Y705), STAT3 and β-actin. The experiment was performed in duplicate with reproducible results. The E884K mutation negatively modulated the effect of L858R to erlotinib inhibition in a dominant manner but enhanced sensitivity of the mutant receptor to gefitinib inhibition. (**b**) Densitometric quantitation of the p-EGFR (Y1068) levels showing differential alteration of sensitivity to erlotinib (more resistant) and gefitinib (more sensitive) by the E884K mutation when in-*cis* with L858R. The densitometric scanning of the p-EGFR immunoblot bands was performed digitally using the NIH ImageJ software program and was normalized to the total EGFR expression levels. (**c**) Relative expression of the apoptotic marker cleaved-PARP(Asp214) in L858R and L858R + E884K *EGFR* variants treated with increasing concentrations of erlotinib (left) and gefitinib (right). The immunoblot from whole cell lysates as in (**a**), using anti-cleaved-PARP(Asp214) (c-PARP) antibody is shown here (above) together with the densitometric quantitation (below) adjusted to β-actin loading control using the NIH ImageJ software program. (**d**) COS-7 cells with stable transduced expression of L858R or L858R + E884K mutant *EGFR* were tested in cellular cytotoxicity assay *in vitro* under drug treatment with either erlotinib or gefitinib at indicated concentrations. Results are shown in percentage change of cell viability of L858R + E884K EGFR-COS-7 compared with the control L858R EGFR-COS-7 cells at each concentration of TKI tested. E884K mutation, when in-*cis* with L858R, significantly decreased the sensitivity of cell viability inhibition by erlotinib compared with L858R alone; however, it significantly increased the sensitivity of cell viability inhibition by gefitinib compared with L858R alone. In the case of erlotinib, E884K was desensitizing to L858R, leading to lower cytotoxicity (56.3 ± 2.68% increased viable cells after inhibition at 5 μM, $P = 0.0004$) compared with L858R alone. Conversely, in gefitinib inhibition, E884K further sensitized L858R in-*cis*, leading to significantly higher cytotoxicity (63.5 ± 6.86% decreased viable cells after inhibition at 5 μM, $P = 0.0013$) compared with L858R alone. Error bar, s.d. ($N = 3$). *$P < 0.05$, compared with L858R alone. Representative photomicrographs of cells after 48 h of indicated inhibitor treatment (5 μM) *in vitro* were included to illustrate the presence of differential cytotoxicity as seen with the nonviable detached cells or cell fragments (× 10). Examples of increased floating nonviable cells are highlighted with arrows.

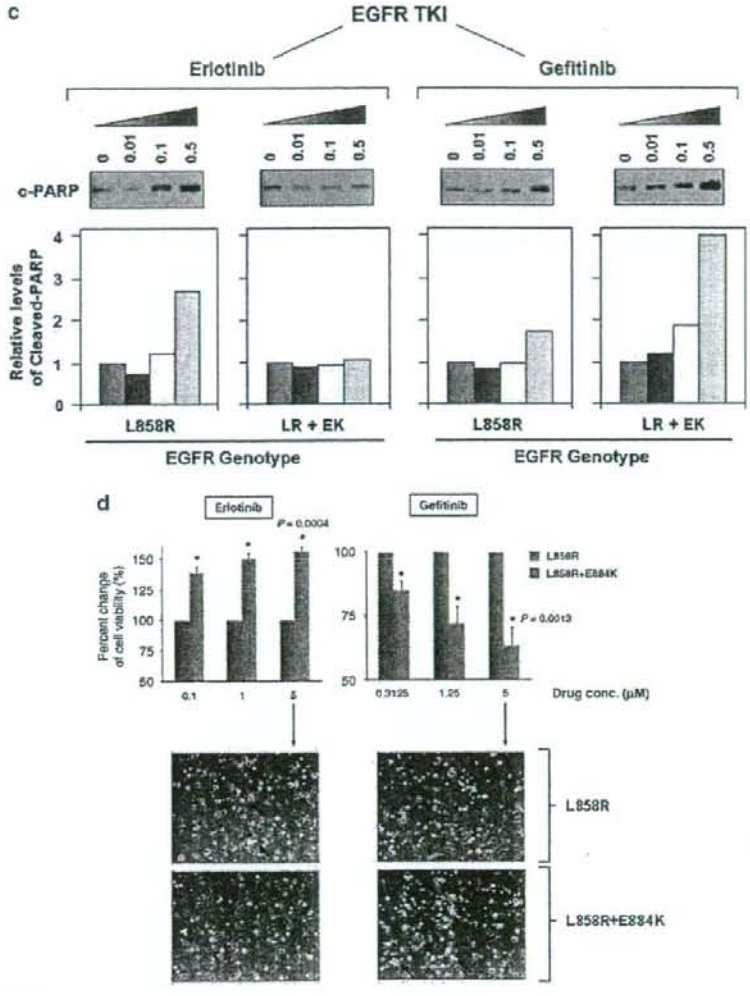

Figure 1 Continued.

(Figure 2). Hence, E884K mutation can work in concert with L858R to modulate mutant receptor sensitivity to different targeted inhibitors. Similarly, E884K further enhanced the sensitivity of L858R to the inhibition by the irreversible EGFR/ERBB2 inhibitor, CL-387,785. On the other hand, the sensitivity of EGFR phosphorylation between the L858R and L858R + E884K EGFR receptors in Tyrphostin-AG1478 (reversible EGFR-TKI), GW583340 (reversible dual EGFR/ERBB2-TKI) and lapatinib (reversible dual EGFR/ERBB2-TKI) did not significantly differ. Hence, the E884K mutation, when in-*cis* with L858R, modulates the sensitivity of the mutant receptor toward ERBB family kinase inhibitors in an inhibitor-specific manner.

E884K is activating, and can work cooperatively with L858R to differentially modulate downstream signal transduction

To address the question whether there are other downstream phosphoproteins that can be differentially activated by the E884K mutation compared with the activating L858R mutation, the global phosphotyrosine profiles of the cellular proteins induced by the mutant EGFR were examined. The E884K alone and L858R + E884K double-mutant EGFR remained sensitive to EGF, and the E884K mutation cooperates with L858R when in-*cis* to further enhance the mutational effects on downstream phosphoprotein activation (data not shown). To date, essentially all mutational combinations involving L858R studied thus far were found to

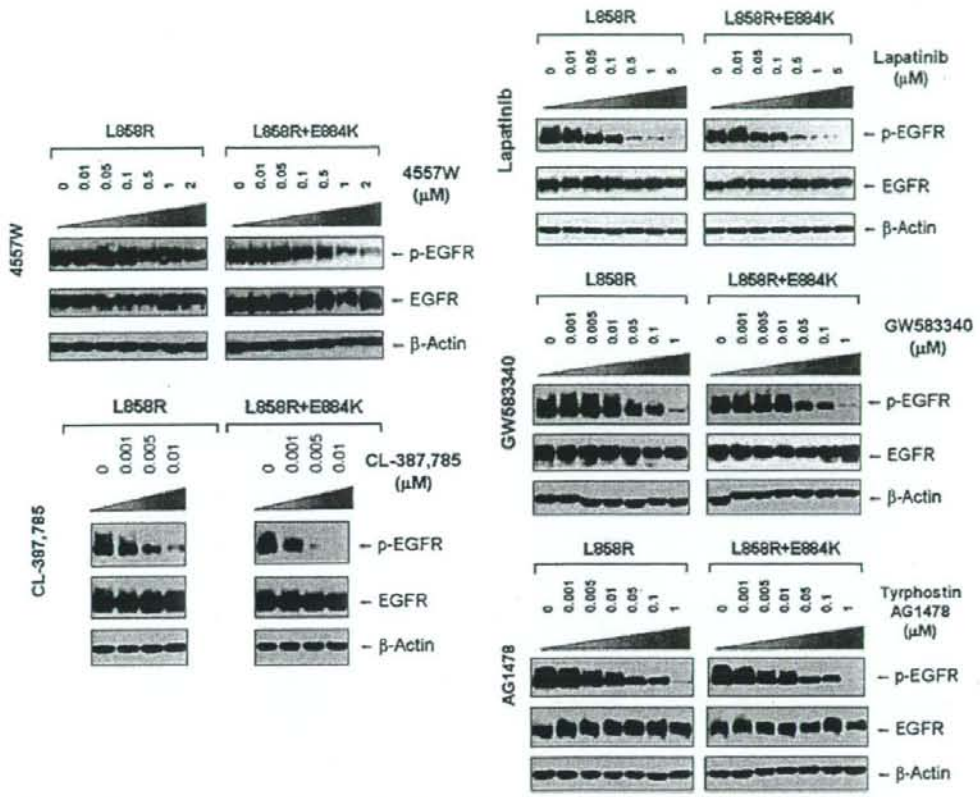

Figure 2 Effects of L858R/E884K-EGFR on other epidermal growth factor receptor (EGFR) kinase inhibitors. The EGFR mutation E884K modulated L858R mutation in-*cis* with inhibitor-specific effects on the sensitivities to EGFR phosphorylation inhibition by the inhibitors (4557W, GW583340, Tyrphostin-AG1478, lapatinib and CL-387,785). Stable COS-7 transfectant cells expressing equivalent levels of the following *EGFR* variants were used: L858R (LR) and L858R + E994K (LR + EK). Cells were cultured in 0.5% bovine serum albumin-containing serum-free media for 16 h, and then treated with or without increasing concentrations of the EGFR TKIs as indicated, in the presence of EGF stimulation (100 ng/ml). Whole cell lysates were extracted for SDS polyacrylamide gel electrophoresis and immunoblotting using the following antibodies: p-EGFR (Y1068), EGFR and β-actin. E884K mutation worked in concert with L858R in-*cis* to enhance the sensitivity of the mutant receptor to inhibition by the kinase inhibitor 4557W, and CL-387,785. On the other hand, it has little effects on the inhibition by lapatinib, GW583340 and Tyrphostin-AG1478.

exist in-*cis*, suggesting potential *cis* mutation-to-mutation cooperation in EGFR signaling and possibly tumorigenesis (Tam *et al*., 2006). To determine the effect of E884K on mutant EGFR signaling, we next studied the EGFR activation of the downstream PI3K-AKT-MAPK (ERK1/2)-STAT pathway. E884K mutant (alone or in-*cis* with L858R) receptor exhibited constitutive activation of the tyrosine phosphorylated EGFR comparable with L858R (Figure 3a). E884K and L858R + E884K mutants remained sensitive to EGF and were activated by the ligand to a level comparable with L858R (Figure 3a). L858R was associated with downstream activation of p-AKT signaling, which was inducible by EGF stimulation. When in-*cis* with L858R, E884K mutation (L858R + E884K) downregulated constitutive AKT phosphorylation. E884K, alone or in-*cis* with L858R, can also mediate constitutive induction of p-STAT3 (pY705) (important for STAT3 dimerization and transcriptional activation of target genes) (Figure 3a). Interestingly, the double mutation L858R + E884K conferred a distinctly more sensitive response to EGF stimulation selectively in the mitogen-activated protein kinase (extracellular signaling-regulated kinase 1/2) (MAPK-ERK1/2) cell proliferation pathway compared with either wild type, E884K alone or L858R alone. Consistent with this differential signaling effect, the L858R + E884K-COS-7 cells had a significantly higher cell proliferation rate than that of the L858R-COS-7 cells in the MTS cell proliferation assay for 5 days (Figure 3b). At days 3 and 5, the cell proliferation rate as determined by % viable cell increase during the assay period was 1.46-fold (day 3) and 1.40-fold ($P = 0.0013$) higher (day 5) in L858R + E884K than L858R alone. L858R + E884K

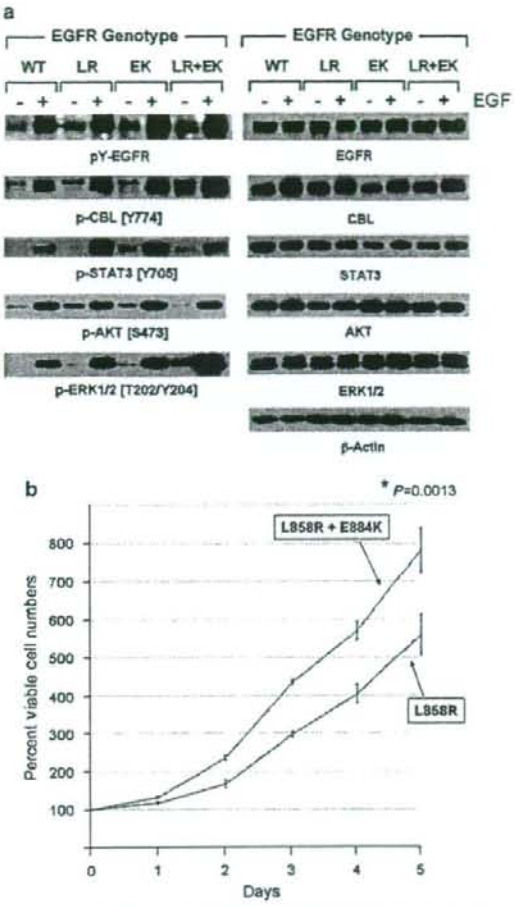

Figure 3 Effects of mutational disruption of the Glu(E)884 Arg(R)958 ion pair in epidermal growth factor receptor (EGFR) signaling. (**a**) Stable COS-7 transfectant cells expressing the various *EGFR* variants were cultured in 0.5% bovine serum albumin-containing serum-free media, followed by EGF stimulation (100 ng/ml, 10 min). Whole cell lysates were prepared for SDS polyacrylamide gel electrophoresis and immunoblotted using the antibodies against: phosphotyrosine (pY-EGFR), EGFR, p-CBL (Y774), CBL, p-STAT3 (Y705), STAT3, p-AKT (S473), AKT, p-ERK1/2 (T202/Y204), ERK1/2 and β-actin. E884K, either alone or in-*cis* with L858R, modulated differential activation of downstream mutant EGFR signaling. (**b**) The EGFR double mutations L858R + E884K conferred a significantly higher cell proliferation rate than L858R alone in the COS-7 cells stably expressing the transduced mutant *EGFR*. Cellular viability assay was performed with the cells growing in regular growth media (10% fetal bovine serum) up to 5 days as described in Materials and methods. The MTS viability assay was performed in triplicate. Error bar, s.d. $^*P = 0.0013$.

also conferred a higher induction of p-CBL as well. Hence, the double mutation L858R + E884K modulated basal and stimulated downstream EGFR signaling differentially with differential effects on the AKT (downregulated), CBL and MAPK-ERK1/2 phosphorylation (upregulated). Moreover, E884K had a dominant effect over L858R, when in-*cis*, in these signaling modulatory effects.

Disruption of a conserved ion pair, Glu(E)884-Arg(R)958, in EGFR differentially alters kinase inhibitor sensitivity

Next, bioinformatics analysis of the E884 residue was performed by multiple kinase domain amino-acid sequence alignments of the human kinome, using the AliBee multiple sequence alignment program (GeneBee, Moscow, Russia) (Supplementary Figure 1). Amino-acid alignments of the kinase domains of phylogenetically diverse groups of kinases such as among the ERBB family, the vascular endothelial growth factor receptor family and the TRK family show that the E884 residue is highly conserved (Figure 4a). In addition, a second residue was also found to be highly conserved (R958) (Figure 4a). Further multiple sequence alignments of 321 human kinase domains show high conservation of both E884 and R958 residues of the EGFR kinase domain (Supplementary Figure 1). The glutamic acid residue (E884) is conserved in >77% and the arginine residue (R958) is conserved in >55% of human kinases in the kinome.

Finally, we mapped the locations of the L858R and E884K mutations onto the three-dimensional structure of the EGFR kinase domain complexed with erlotinib and with lapatinib (PDB accession codes 1M17 (Stamos *et al*., 2002) and 1XKK (Wood *et al*., 2004)) (Figure 4b). We also generated a superposition of the EGFR kinase domain with multiple diverse kinase catalytic domains (Figure 4c). These analyses show the structural conservation of the buried Glu(E)-Arg(R) ion pair and that the exon 22 residue, E884, is physically distant from L858 in exon 21. Furthermore, unlike L858, E884 is not proximal to the adenosine triphosphate-binding cleft of the kinase domain, making it difficult to predict its effects on kinase inhibitor interactions. Mutation of the acidic glutamate residue at codon 884 to a basic lysine will disrupt the highly conserved ion pair through charge–charge repulsion with the basic residue R958 (Figures 4b and c).

To further test the hypothesis of the disruption of the conserved E884–R958 salt bridge as a mechanism underlying the differential response of the mutant EGFR to kinase inhibitors, we tested the double mutant L858R + R958D against erlotinib and gefitinib (Figure 5). Substitution of the wild-type Arg(R)958 with Asp(D)958 was created using site-directed mutagenesis. We hypothesized that the R958D substitution would disrupt the ion pair with E884 through electrostatic repulsion, in a way similar to the effect of the E884K substitution. COS-7 cells transfected to express the indicated mutant EGFR receptors were inhibited using either erlotinib or gefitinib *in vitro* with increasing concentrations. Similar to E884K, R958D modulated the sensitizing effect of L858R differentially to reversible EGFR inhibitors when in-*cis* (with L858R). R958D mutation, when in-*cis* with L858R, decreased the

sensitivity of the mutant receptor to erlotinib inhibition, while increasing the sensitivity to gefitinib in a dominant manner (Figures 5a and b).

Mutational disruption of the conserved kinase ion pair in MET kinase by E1271K-MET also differentially alters the sensitivity of phosphorylation inhibition by MET inhibitors

MET has been shown to play a key role in the development of many human malignancies. A number of mutations have been identified in *MET* from various cancers. Recently, it has been shown that MET represents a key oncogenic signaling in lung cancer alongside with EGFR signaling (Rikova *et al.*, 2007; Guo *et al.*, 2008; Tang *et al.*, 2008). Moreover, MET can cross-activate with EGFR when they are co-expressed, which happens rather frequently (Rikova *et al.*, 2007; Tang *et al.*, 2008). MET has also been shown to be an attractive therapeutic molecular target (Ma *et al.*, 2003b; Shinomiya *et al.*, 2004; Mazzone and Comoglio, 2006; Peruzzi and Bottaro, 2006; Smolen *et al.*, 2006). Here, we test the hypothesis that E1271K mutation of *MET*, analogous to E884K-*EGFR*, can also differentially alter inhibitory sensitivity toward selective MET inhibitors (Figure 6). The Glu(E)1271-Arg(R)1345 constitutes the conversed ion-pair in MET kinase (Figures 4 and 6). The location of the E1271–R1234 ion pair in MET kinase is illustrated in the recently reported crystallographic structure of the MET kinase domain complexed with SU11274 (Bellon *et al.*,

Figure 4 The ion pair Glu(E)884-Arg(R)958 in the epidermal growth factor receptor (EGFR) kinase domain is a highly conserved feature in the human kinome. (a) A selected list of 32 diverse human protein kinases with known importance as validated or potential cancer therapeutic targets was included here with bioinformatics alignment analysis of the kinase domain amino-acid sequences. Glu884 (E884) and Arg958 (R958) of EGFR are both highly conserved residues among these kinases. (Left) Amino-acid alignment of the kinase domains of 32 diverse members of human protein kinases showing E884-EGFR is highly conserved: EGFR, ERBB2, ERBB3, ERBB4, RON, MET, TYRO3, MER, AXL, RYK, RET, FGFR1, FGFR2, FGFR3, FLT3, KIT, PDGFR-A, PDGFR-B, vascular endothelial growth factor receptor-1, vascular endothelial growth factor receptor-2, vascular endothelial growth factor receptor-3, SRC, EPHA2, EPHB2, FAK, ZAP70, TRK-A, TRK-B, TRK-C, IGFR1, ALK and c-ABL. (Right) R958-EGFR is also highly conserved among diverse members of kinases. For the complete alignment analysis of kinase domains of the human kinome, see Supplementary Figure 1. (b) EGFR kinase domain crystal structures (PDB accession codes 1M17 (Stamos *et al.*, 2002) and 1XKK (Wood *et al.*, 2004)) when in complex with erlotinib (blue) and lapatinib (green) are shown. The locations of L858 (exon 21) and E884 (exon 22) are highlighted. E884 (acidic) and R958 (basic) residues form an ion pair in wild-type EGFR that would be disrupted by the E884K substitution from the acidic glutamic acid (E) to the basic lysine (K). The E884 R958 salt bridge is present in the kinase domain crystal structures complexed to either erlotinib or lapatinib. (c) Superposition of the EGFR kinase domain with the catalytic domains of diverse kinases shows structural conservation of a buried Glu(E) Arg(R) ion pair. The crystal structure of EGFR tyrosine kinase (PDB accession code: 1M17) (Stamos *et al.*, 2002) was superimposed with the catalytic kinase domains of human CDK2 (PDB accession code: 1VYW) (Pevarello *et al.*, 2004), human JNK3 (PDB accession code: 1PMQ) (Scapin *et al.*, 2003), human insulin receptor kinase (PDB accession code: 1IR3) (Hubbard, 1997), ZAP-70 tyrosine kinase (PDB accession code: 1U59) (Jin *et al.*, 2004), LCK kinase (PDB accession code: 1QPD) (Zhu *et al.*, 1999) and MET (PDB accession code: 2RFS) (Bellon *et al.*, 2008) using Cα atoms in the program DeepView/Swiss-PdbViewer v3.7. The conserved Glu Arg ion pair is shown in stick format, with oxygen atoms colored red and nitrogens, blue. The EGFR side chains are shown in yellow. The structural location of the ion pair is conserved in these crystal structures and helps orientate helix αEF. Figures 4b and c were prepared using the program PYMOL (www.pymol.org).

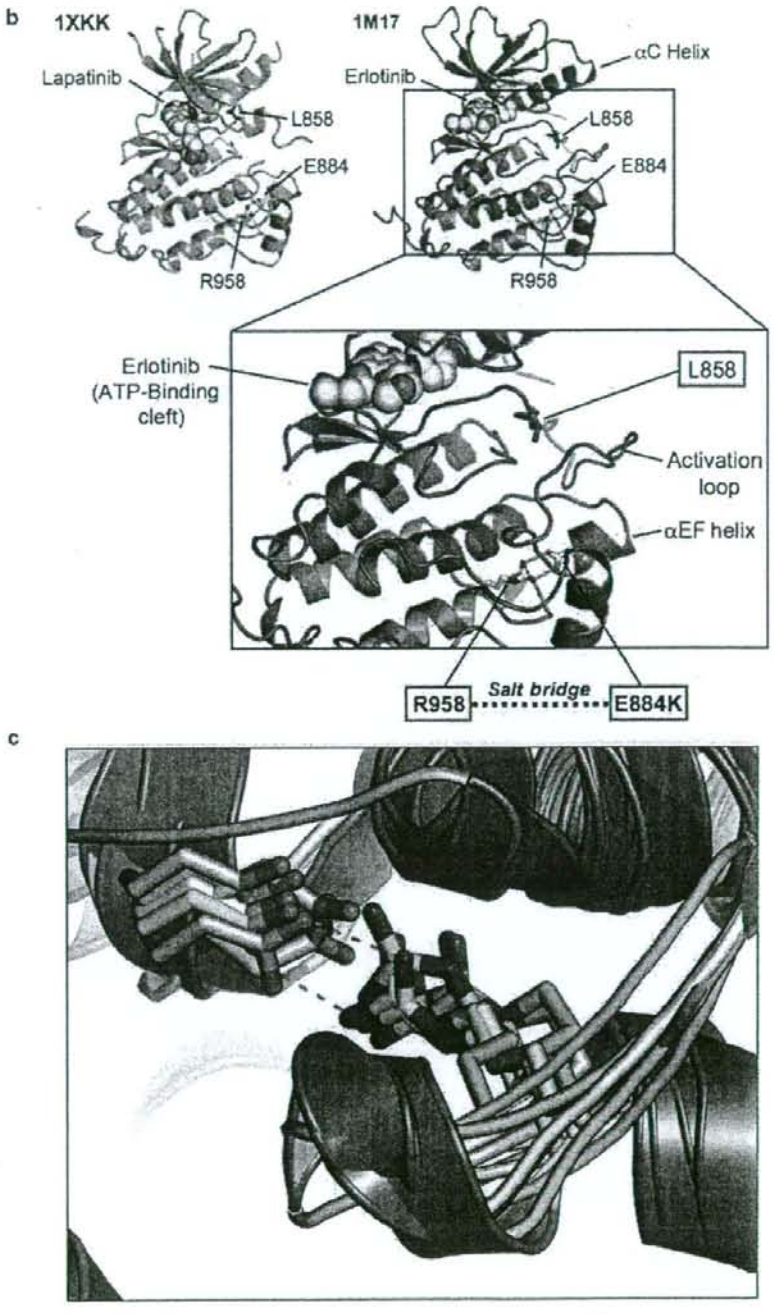

Figure 4 Continued.

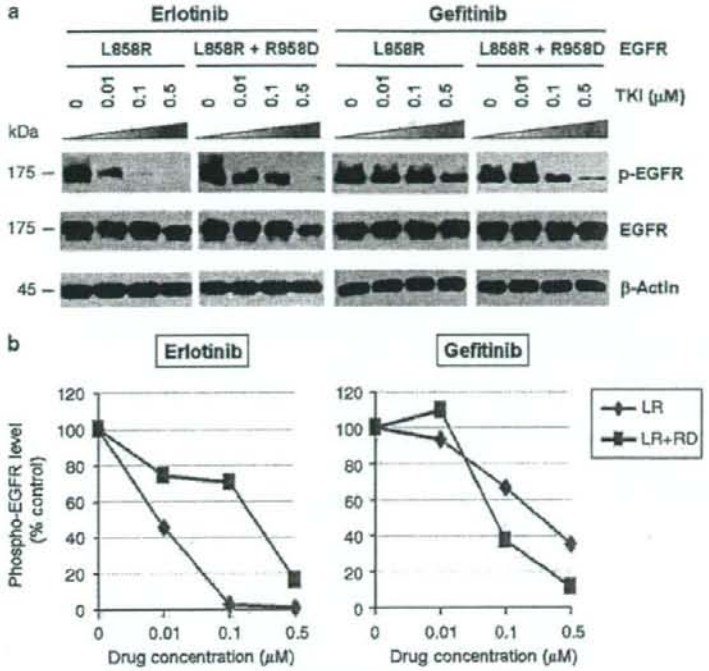

Figure 5 Disruption of the conserved Glu(E)884 Arg(R)958 salt bridge by a R958D substitution differentially altered L858R mutant receptor sensitivity to epidermal growth factor receptor (EGFR) inhibitors. (a) Stable COS-7 transfects expressing the sensitizing L858R and double-mutant L858R + R958D variants of EGFR were cultured in 0.5% bovine serum albumin-containing serum-free media for 16 h, and then incubated with increasing concentrations of either erlotinib or gefitinib, in the presence of EGF stimulation (100 ng/ml). Whole-cell lysates were extracted for SDS polyacrylamide gel electrophoresis and immunoblotted using antibodies against the followings: p-EGFR (Y1068), EGFR and β-actin. R958D mutation modulated the effect of L858R on inhibitor sensitivity resulting in desensitization of the mutant receptor to erlotinib inhibition but modestly enhanced sensitivity to gefitinib inhibition. (b) Densitometric quantitation of the p-EGFR (Y1068) levels showing that R958D mutation differentially altered L858R mutant receptor sensitivity to erlotinib (more resistant) and gefitinib (more sensitive). Densitometric scanning of the immunoblot signals shown in (a) was performed using NIH ImageJ software program, with normalization to total EGFR expression levels.

2008). Stable COS-7 transfectant cells expressing similar levels of wild type and E1271K-*MET* were used in this experiment using the two reversible preclinical MET inhibitors SU11274 (Ma *et al.*, 2005a) and PHA665752 (Ma *et al.*, 2005a, b). We did not find any significant modulation of sensitivity to SU11274 inhibition in the E1271K-MET cells (Figure 6b). On the other hand, the E1271K mutation of MET enhanced the sensitivity of inhibition by PHA665752 in the phosphorylation of the mutant MET at its major autophosphorylation sites (pY1234/1235) (equivalent to pY1252/1253 phosphosites as in the full-length *MET* transcript, with a difference of 18 amino acids in the exon 10 with the common alternatively spliced variant) in the kinase domain, and its downstream signaling proteins AKT and ERK1/2 (Figure 6b). Hence, disrupting the MET kinase salt bridge by the E1271K mutation also differentially alters sensitivity to MET kinase inhibitors in an inhibitor-specific manner.

Mutations at the conserved Glu(E)–Arg(R) ion pair in the human kinome

As the E884K somatic mutation was originally identified in a never-smoker woman of Japanese descent, we performed mutational screening for the presence of mutation at the E884 and R958 residues of *EGFR* among a cohort of 67 lung tumor genomic DNA specimens from Japanese non-small-cell lung cancer patients (including 66 transbronchial biopsies and 1 surgical specimen). Nonsynonymous mutations were not present in either residue location in this patient cohort. On the basis of our results suggesting the conserved structure and function of the Glu(E)–Arg(R) ion pair in EGFR and among other kinases in the kinome, we hypothesized that there would be other cancer-associated mutations at the conserved ion pair within the human kinome in kinases other than EGFR. Here, we performed bioinformatics survey of the updated Catalog of Somatic Mutations In Cancer (COSMIC) database (http://www.sanger.ac.uk/genetics/CGP/cosmic/) containing

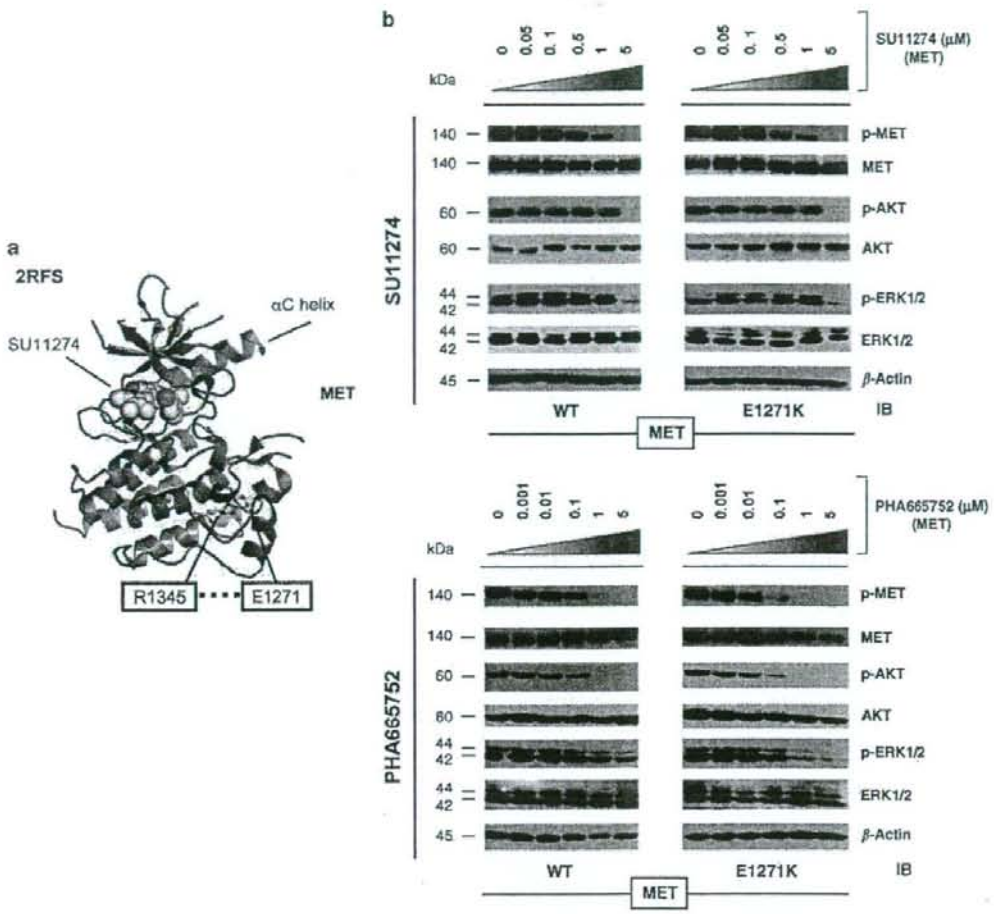

Figure 6 Mutational disruption of the conserved E1271 R1345 ion pair in MET kinase salt bridge causes inhibitor-specific modulation of sensitivity to SU11274 (unchanged) and PHA665752 (more sensitive). (a) MET kinase domain crystal structure (PDB accession code: 2RFS) (Bellon *et al*., 2008) highlighting the salt bridge between E1271 and R1345. Crystal structure solved in complex with SU11274 is shown. The conserved Glu Arg ion pair is shown in stick format, with oxygen atoms colored red, nitrogen atoms colored blue and carbon atoms colored yellow. This figure was prepared using the program PYMOL (www.pymol.org). (b) Stable COS-7 transfects expressing E1271K mutant *MET* were cultured in 0.5% bovine serum albumin-containing serum-free media for 16 h, then incubated with increasing concentrations of the MET inhibitors SU11274 (top) and PHA665752 (bottom) as indicated, in the presence of HGF stimulation (50 ng/ml). Whole-cell lysates were extracted for immunoblotting using antibodies against p-MET (Y1234/Y1235), MET, p-AKT, AKT, p-ERK1/2, ERK1/2 and β-actin. Wild-type *MET*-expressing COS-7 transfectant cells were included as control. E1271K mutation of MET increased the sensitivity of MET kinase phosphorylation inhibition by PHA665752.

somatic mutations identified in kinases among human cancers (Figure 7). We have conducted a complete and comprehensive survey throughout the entire human kinome for mutations identified at the conserved Glu(E)–Arg(R) ion pair in COSMIC. We also documented here the hits identifying mutations clustered in the vicinity of the ion pair, 30 amino acids proximal or distal to the Glu(E) or Arg(R). Interestingly, several kinases within the kinome were found to have mutations occurred at the Glu(E) residue, homologous to the E884–EGFR residue. These include KIT (E839K), RET (E921K), STK11/LKB1 (E223*). These are all known cancer-associated kinases that have dysregulated signaling in various human cancers, including GIST and hematological malignancies (KIT), papillary thyroid cancer (multiple endocrine neoplasm syndrome type 2) (RET) and lung cancer (RET, LKB1).

Discussion

In the era of molecularly targeted therapeutics in cancer therapy, the impact of cancer-associated mutations on kinase inhibitor sensitivity-resistance has increasingly

A[a]

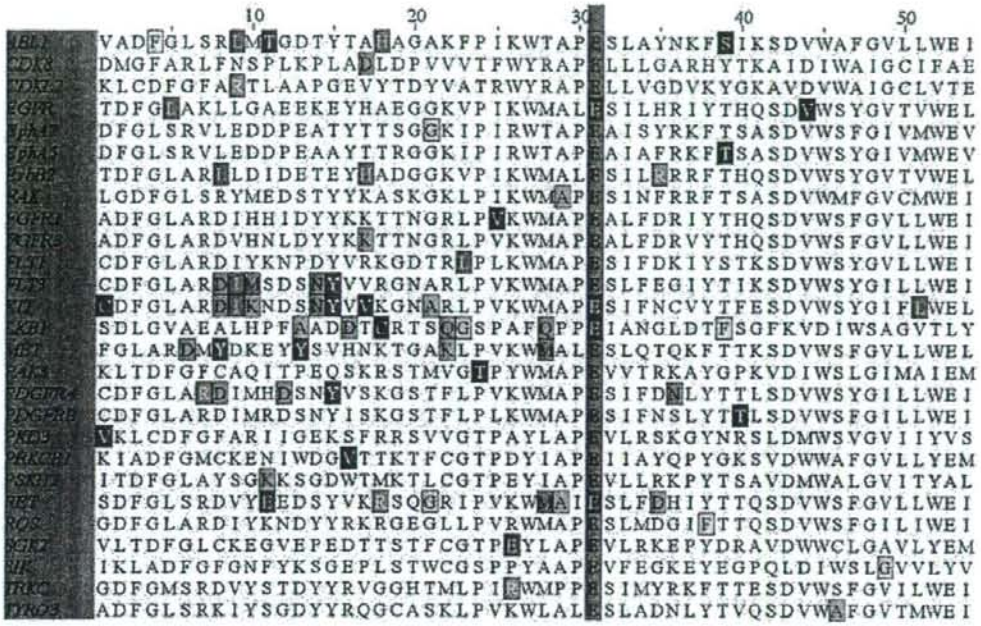

b

GENES	Mutations
ABL1:	F382L, L387M, T389A, H396P, H396R, S417Y
CDK8:	D189N
CDKL2:	R149Q
EGFR:	L858R, ***E884K***, V897I
EPHA2:	G777S
EPHA5:	T856I
ERBB2:	L869Q, H878Y, R896C
FAK:	***A612V***
FGFR1:	V664L
FGFR3:	K650E, K650M, K650Q, K650T
FLT1:	L1061V
FLT3:	D835E, D835F, D835H, D835N, D835V, D835Y, I836F, I836M, I836S, M837P, N841H, N841K, Y842C
KIT:	C809G, C809R, A814S, A814T, D816A, D816E, D816F, D816G, D816H, D816I, D816N, D816V, D816Y, I817V, K818R, D820E, D820G, D820H, D820N, D820V, D820Y, N822H, N822K, N822T, N822Y, Y823C, Y823D, Y823N, V825A, V825I, A829P, ***E839K***, L859P
LKB1:	A205T, D208N, C210*, Q214*, G215D, ***Q220****, ***E223****, F231L
MET:	D1246H, Y1248C, Y1248H, Y1253D, K1262R, ***M1268I***, ***M1268T***
PAK3:	T425S
PDGFRA:	R841S, D842*, D842I, D842V, D842Y, D846Y, Y849C, N870S
PDGFRB:	T882I
PKD3:	V716M
PRKCB1:	V496M
PSKH2:	K212I
RET:	E901K, R908K, G911D, ***M918T***, ***A919V***, ***E921K***, D925H
ROS:	F2138S
SGK2:	E259K
SIK:	G211S
TRKC:	R721F
TYRO3:	A709T

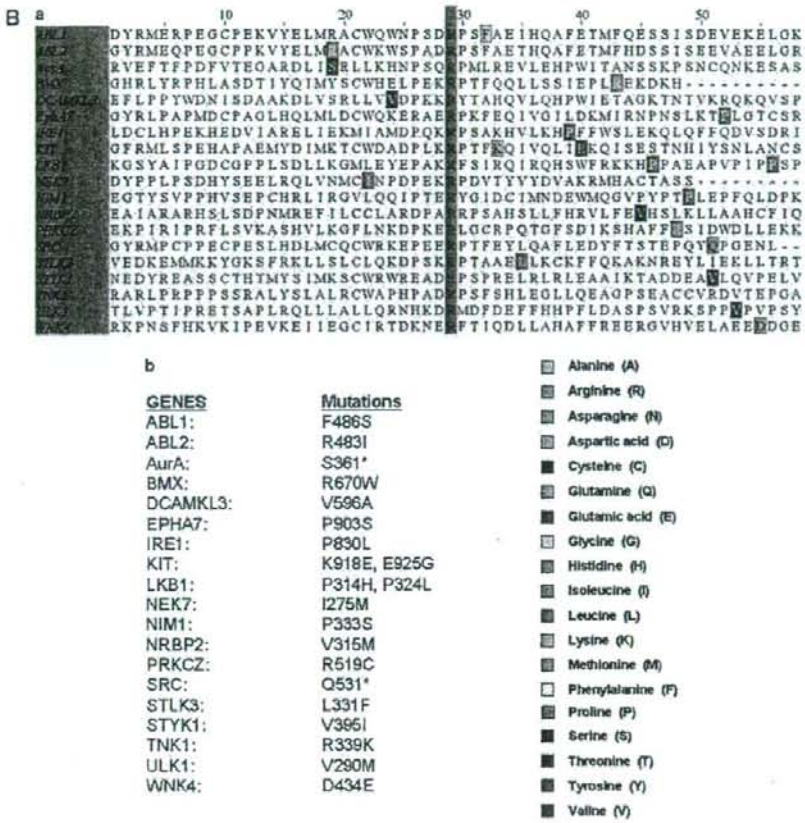

Figure 7 Continued.

important implications in the success of novel targeted inhibitors such as erlotinib (EGFR-TKI). Furthermore, knowledge of mutational correlation with inhibitor sensitivity-resistance would most likely facilitate more effective and 'personalized' targeted therapeutics development in cancer therapy. The clinical course of the patient where the somatic E884K mutation was identified (Choong *et al*., 2006) suggested that different mutations of a target kinase, such as EGFR, may lead to differential responses to targeted kinase inhibitors. Alternatively, one may postulate that there might be differences in cerebrospinal fluid penetrance by TKIs that could potentially account for central nervous system failure with disease progression in the compartment on therapy (Jackman *et al*., 2006). Our biochemical studies here now show that E884K mutation in-*cis* with L858R differentially altered inhibitor sensitivity when compared with L858R alone, through differential inhibition of the pro-survival AKT and STAT3 signaling pathways associated with altered induction of cleaved-PARP(Asp214). This is also shown to occur in an inhibitor-specific manner within the class of various

Figure 7 Survey of identified mutations at the conserved salt bridge ion pair in the human kinome (COSMIC). The COSMIC database for the human cancer genome resequencing was surveyed and screened for potential mutations identified at or near the conserved Glu(E) Arg(R) salt bridge ion pair in the human kinome. (**A**) (a) Glu(E)884-EGFR and analogous alignment in the kinome. (b) List of the mutations identified in the kinome is included as reference. (**B**) (a) Arg(R)958-EGFR and analogous alignment in the kinome. (b) List of the mutations identified in the kinome is included as reference. The color code for the amino acids is included here. We have identified several kinases within the kinome that have mutations occurred at the Glu (E) residue, homologous to the E884-EGFR. These include KIT (E839K), RET (E921K) and LKB1 (E223*). These are all known oncogenic kinases that have dysregulated signaling in various human cancers, including GIST and hematological malignancies (KIT), papillary thyroid cancer (multiple endocrine neoplasm syndrome type 2) (RET) and lung adenocarcinoma (RET, LKB1). Whereas *KIT* and *RET* are oncogenes, *LKB1* has been shown to be a tumor-suppressor gene in lung cancer, and here we showed clustering of truncation mutations at and near the salt bridge ion pair as a result of a number of mostly nonsense mutations among some missense mutations. Although no mutation at E1271-*MET* was found, there are frequent clustered hotspots of mutations at its close vicinity: three amino-acid residues proximally at M1268 (M1268T/I). This is a known activating mutation of *MET* frequently associated with metastatic lesions promoting tumor motility and progression. The selected kinases with positive 'mutational hits' in our kinome bioinformatics screen are shown here for illustration.

ERBB family small-molecule inhibitors, including reversible single EGFR or dual inhibitors (gefitinib, erlotinib, lapatinib, 4557W, GW583340 and Tyrphostin-AG1478) and irreversible EGFR inhibitor (CL-387,785).

Moreover, the E884K alone and L858R + E884K double-mutant EGFR remained sensitive to EGF, and the E884K mutation cooperates with L858R when in-*cis* to enhance the mutational effects on downstream phosphoprotein activation. To date, essentially all mutational combinations involving L858R studied were found to exist in-*cis*, suggesting potential *cis* mutation-to-mutation cooperation in EGFR signaling and possibly tumorigenesis (Tam *et al.*, 2006). Interestingly, the double mutation L858R + E884K conferred a distinctly more sensitive response to EGF stimulation selectively in the MAPK-ERK1/2 cell proliferation pathway compared with either wild type, E884K alone or L858R alone. Hence, the double mutation L858R + E884K modulated downstream EGFR signaling differentially with distinctly different effects on the AKT (downregulated) and MAPK-ERK1/2 phosphorylation (upregulated). Moreover, E884K had a dominant effect over L858R, when in-*cis*, in these signaling modulatory effects. E884K, alone or in-*cis* with L858R, can also mediate induction of p-STAT3 (pY705) (important for STAT3 dimerization and transcriptional activation of target genes) and may have a role in differential regulation of STAT3 activation and thus nuclear translocation for transcriptional activity (Lo *et al.*, 2005). Our data also share some similarities to the recent findings that various activating 'gain-of-function' mutations of FLT3 showed differential downstream signaling activation along the STAT3, STAT5, AKT and MAPK-ERK1/2 pathways, whereas all induced FLT3 kinase activation constitutively (Frohling *et al.*, 2007). *EGFR* somatic doublet mutations are potentially more frequent than understood previously, with majority of them representing driver/driver mutations rather than driver/passenger mutations (Chen *et al.*, 2008). Future kinome-targeted therapies should take into account oncogenic effects of doublet mutations in the targets, and detailed analysis of the identified doublet mutations would be warranted.

Through sequence bioinformatics and structural analysis, we identified that the E884–R958 ion pair in EGFR kinase domain is highly conserved, by both sequence homology and structural salt-bridge formation, across the entire human kinome. Many of the protein kinases in the human kinome are 'druggable' therapeutic targets for various human cancers (Krause and Van Etten, 2005; Ma *et al.*, 2005a). This striking finding provides a structural basis for the potential mechanism of alteration of substrate specificity. This hypothesis is substantiated by our study using mutational disruption of the E884–R958 ion pair through an R958D substitution resulting in an opposite electrostatic charge between the wild-type and the mutant residue at codon 958. Similar differential sensitivity toward gefitinib (more sensitive) and erlotinib (more resistant) was observed in our *in vitro* EGFR inhibition study here. It is interesting to note that this salt bridge is located directly between two regions critical for normal EGFR activation, the intermolecular EGFR activation interface and the activation loop. Residue R958 falls between helices αH and αI and is proximal to the intermolecular EGFR activation interface recently revealed by structure-directed studies (Zhang *et al.*, 2006). Residue E884 is the conserved glutamate of the MALE motif (MAPE in PKA) and falls within helix αEF at the C terminus of the activation loop. This salt bridge helps to orientate helix αEF. In the recent EGFR kinase domain crystal structure bound to a peptide substrate analog (PDB accession code: 2GS6) (Zhang *et al.*, 2006), helix αEF packs against the substrate analog, suggesting that disruption of the salt bridge by an acquired E884K mutation could influence substrate recognition and binding. The acquisition of a lysine at codon 884 may therefore bring about local conformation disruptions that alter EGFR interactions with downstream substrates. Although we did not identify further E884K mutation (or any mutations involving R958 residue) in *EGFR* from the Japanese patients tumor sample cohort, the results of our study may have implication on the potential impact of cancer-associated mutations that may interrupt the integrity of the salt bridge of a kinase. As the human kinome is a rich source of 'druggable' targets, we extended our search through bioinformatics data-mining from the COSMIC human cancer genome resequencing project. To this end, we identified several proximal ion pair residue substitutions recorded in the COSMIC database at the E884 (EGFR) homologous residue, in the oncogenic kinases KIT and RET as well as in the tumor-suppressor LKB1 (also known as STK11). Mutations at the neighboring residues of the conserved motif MAPE(884), as exemplified in FAK-A612V, MET-M1268I/T, RET-M918T and RET-A919V, as well as the truncational nonsense mutation in LKB1-Q220*, were also identified from the COSMIC database. Furthermore, the juxtaposing proximal region to the MAPE(884) conserved motif in the kinome also appears to harbor mutational hotspots in the human cancer genome. Nonetheless, the significance of these mutations with respect to the kinase structure and signaling function is not clear. Although KIT has been extensively characterized with an established oncogenic role in some hematological malignancies and GIST, it has not been found to play a key role in lung cancer. However, recent studies have implicated interesting oncogenic role of RET (Thomas *et al.*, 2007), FAK (Ma *et al.*, 2007; Rikova *et al.*, 2007), MET (Ma *et al.*, 2005a) and tumor-suppressor role of LKB1 (Ji *et al.*, 2007) in lung cancer.

Recently, better understanding of signaling network interactions between EGFR and MET is beginning to emerge (Guo *et al.*, 2008; Tang *et al.*, 2008). MET genomic oncogenic amplification has also been identified to correlate with acquired resistance to EGFR inhibitors (gefitinib/erlotinib) with or without T790M-*EGFR* mutation (Bean *et al.*, 2007; Engelman *et al.*, 2007). Numerous kinase domain mutations of *MET* have been identified in previous studies, many of them shown to be activating and most frequently found in

metastatic tumor lesions compared with the primaries (Di Renzo *et al.*, 2000). The E1271–MET conserved ion pair residue occurs within the conserved MALE motif, where M1268 is a mutational hotspot frequently found substituted in human cancers (M1268T/I). This is a known activating mutation of *MET* frequently associated with metastatic lesions promoting tumor motility and progression. Our results here demonstrate that E1271K-MET effectuated differential effect on sensitivity toward the two preclinical MET inhibitors, SU11274 (unchanged) and PHA665752 (sensitizing). Hence, mutations in the kinase domain of MET may play a role in modulating the inhibitory spectrum of MET inhibitors, similar to what is established in EGFR-targeted therapy using gefitinib/erlotinib. Whether these mutationally specific differences in inhibitor sensitivity would eventually be clinically relevant is not clear at present and should be a focus of future research. MET is emerging as an important therapeutic target in cancer therapy beyond EGFR. More detailed studies to better define the relative role of kinase mutations in *MET* and how they can modulate inhibitor sensitivity would be warranted. Furthermore, nonkinase mutations of *MET*, in the extracellular sema domain and the short cytoplasmic juxtamembrane domain, have been identified to be important in lung cancer and mesothelioma (Ma *et al.*, 2003a, 2005a; Jagadeeswaran *et al.*, 2006). Little is known about the correlation of inhibitor sensitivity with these nonkinase mutations, and they should be included in future studies. Bellon *et al.* (2008) recently compared the crystal structures of a novel MET inhibitor AM7, and that of SU11274 when bound to the unphosphorylated form of MET kinase. They identified a novel binding mode of a MET inhibitor AM7 compared with SU11274 and raised the possibility of designing TKIs that have improved specific activity and specificity toward different mutant profiles in different cancers; hence 'mutationally-targeted inhibitors'.

Although the role of kinase domain mutations in modulating the sensitivity-resistance to small-molecule inhibitors, in the case of BCR/ABL, KIT and EGFR, has been quite extensively studied, in-depth understanding of the relative role of mutations in other target kinases, such as MET, RET and FAK in determining specific inhibitor sensitivity is still largely lacking. The ion pair formed by residues E884 and R958 in the EGFR kinase domain is a highly conserved feature in the human kinome, and mutations of this conserved ion pair may result in conformational changes that alter kinase substrate recognition. The discovery that disruption of the conserved E884–R958 ion pair affects EGFR signal transduction and inhibitor sensitivity indicates the clinical importance of *in vitro* and biochemical analysis for all documented resistance mutations. Our analysis also suggests that targeted therapy using small-molecule inhibitors should take into account potential cooperative effects of multiple intramolecular kinase mutations. As the number of targeted TKIs available increases, it is anticipated that a 'personalized' approach to cancer therapy on the basis of knowledge of the activating mutations present should improve the efficacy of these treatments.

Materials and methods

Plasmid constructs and site-directed mutagenesis
The plasmids pcDNA3.1 containing the full-length wild-type *EGFR* and the L858R-*EGFR* cDNA insert was a generous gift from Dr Stanley Lipkowitz (NIH/NCI). The generation of the kinase domain missense mutations of *EGFR*, E884K, L858R + E884K and L858R + R958D were performed using the QuikChange Site-Directed Mutagenesis XL II kit (Stratagene, La Jolla, CA, USA) as described previously (Choong *et al.*, 2006). The E1271K mutation of *MET* was introduced into the wild-type *MET* plasmid (Ma *et al.*, 2003a). Incorporation of the correct mutations was confirmed by direct DNA sequencing of the constructs.

Cell culture and transfection
COS-7 cells were grown as described previously (Choong *et al.*, 2006). Transfection method was described in Supplementary Materials and methods.

Cell proliferation and cytotoxicity assays
Cell proliferation and cytotoxicity assays were performed using tetrazolium compound-based CellTiter 96 AQ_{ueous} One Solution Cell Proliferation (MTS) assay (Promega) (see Supplementary Materials and methods).

Preparation of cell lysates and immunoblotting
Whole-cell lysates were extracted, separated by 7.5% SDS–polyacrylamide gel electrophoresis , immunoblotted using the various primary antibodies indicated and developed with SuperSignal West Pico Chemiluminescent Substrate (Pierce, Rockford, IL, USA) as described previously (Choong *et al.*, 2006). The following primary antibodies were used: phosphotyrosine (4G10, Upstate Biotechnology, Lake Placid, NY, USA), phospho-EGFR (Y1068) (BioSource International, Camarillo, CA, USA), EGFR (Santa Cruz Biotechnology, Santa Cruz, CA, USA), phospho-STAT3 (Y705) (Cell Signaling, Danvers, MA, USA), STAT3 (Zymed, South San Francisco, CA, USA), phospho-AKT (S473) (Cell Signaling), AKT (Biosource International), phospho-ERK1/2 (T202/Y204) (Cell Signaling), ERK1/2 (Biosource International), cleaved-PARP(Asp214) (cleaved-poly (ADP-ribose) polymerase (Asp214)) (Cell Signaling) and β-actin (Santa Cruz Biotechnology).

Chemicals
The details regarding the EGFR TKIs and MET TKIs used in this study are described in the Supplementary Materials and methods.

Lung tumor genomic DNA extraction and DNA sequencing
Genomics DNA was extracted using standard techniques from 67 non-small-cell lung cancer patients treated from July 1995 to March 2003 at Osaka Prefectural Medical Center for Respiratory and Allergic Disease (Osaka, Japan). All tumor samples were used in accordance with Institutional Review Board protocol, with patients' informed consent wherever necessary. Screening for mutations within exon 22 (harboring E884) and exon 23 (harboring R958) was performed using standard single-strand conformational polymorphism analysis, followed by direct DNA sequencing when indicated (for details, see Supplementary Materials and methods).

Bioinformatics sequence analysis

Multiple sequence alignments of kinase domains in the human kinome were performed for 321 human kinase domains. The positions of the conserved glutamate (E) and arginine (R) residues are colored purple and those of EGFR are indicated in red. FASTA files for human kinase domains were obtained from the kinase database at Sugen/Salk (Kinbase, La Jolla, CA, USA) and aligned with the AliBee multiple sequence alignment program (GeneBee) (Brodsky *et al.*, 1992) using Clustal format. Resulting alignments were colored using JalView 2.2 (Clamp *et al.*, 2004) according to sequence conservation (BLOSUM62). In addition, the amino-acid sequences from a selected list of 32 diverse human protein kinases were obtained from the ENSEMBL database (www.ensembl.org). The amino-acid sequences of these kinase domains were analysed and aligned using the EMBL-EBI online CLUSTALW software (www.ebi.ac.uk/clustalw).

Structural analysis

EGFR crystal structures (PDB accession codes 1M17, 1XKK and 2GS6) (Stamos *et al.*, 2002; Wood *et al.*, 2004; Zhang *et al.*, 2006) were analysed using the program O (Jones *et al.*, 1991). Superposition of the EGFR kinase domain with the catalytic domains of diverse kinases was performed to study the structural conservation of a buried Glu(E)–Arg(R) ion pair. The crystal structure of EGFR tyrosine kinase (PDB accession code: 1M17) (Stamos *et al.*, 2002) was superimposed with the catalytic kinase domains of human CDK2 (PDB accession code: 1VYW) (Pevarello *et al.*, 2004), human JNK3 (PDB accession code: 1PMQ) (Scapin *et al.*, 2003), human insulin receptor kinase (PDB accession code: 1IR3) (Hubbard, 1997), ZAP-70 tyrosine kinase (PDB accession code: 1U59) (Jin *et al.*, 2004), LCK kinase (PDB accession code: 1QPD) (Zhu *et al.*, 1999) and MET (PDB accession code: 2RFS) (Bellon *et al.*, 2008) using Cα atoms in the program DeepView/Swiss-PdbViewer v3.7. Figures were prepared using the program PYMOL (www.pymol.org).

Abbreviations

COSMIC, catalogue of somatic mutations in cancer; EGFR, epidermal growth factor receptor; MAPK (ERK1/2), mitogen-activated protein kinase (extracellular signaling-regulated kinase 1/2); STAT3, signal transducer and activator of transcription 3; TKI, tyrosine kinase inhibitor.

Acknowledgements

Patrick C Ma is supported by NIH/National Cancer Institute-K08 Career Development Award (5K08CA102545-04), American Cancer Society (Ohio)-Institutional Research Grant (IRG-91-022, Case Comprehensive Cancer Center) and Ohio Cancer Research Associates (Give New Ideas A Chance) Grant Award. Titus J Boggon is an American Society of Hematology Junior Faculty Scholar. Edward T Petri is supported by an NIH/National Cancer Institute T32 training Grant (5T32CA009085-32). We thank Dr Zhenghe J Wang (Department of Genetics, Case Western Reserve University) for critically reading the manuscript and for helpful suggestions.

References

Bean J, Brennan C, Shih JY, Riely G, Viale A, Wang L *et al.* (2007). MET amplification occurs with or without T790M mutations in EGFR mutant lung tumors with acquired resistance to gefitinib or erlotinib. *Proc Natl Acad Sci USA* **104**: 20932 20937.

Bellon SF, Kaplan-Lefko P, Yang Y, Zhang Y, Moriguchi J, Rex K *et al.* (2008). c-Met inhibitors with novel binding mode show activity against several hereditary papillary renal cell carcinoma related mutations. *J Biol Chem* **283**: 2675 2683.

Brodsky LI, Vasiliev AV, Kalaidzidis YL, Osipov YS, Tatuzov RL, Feranchuk SI. (1992). GeneBee: the program package for biopolymer structure analysis. *Dimacs* **8**: 127 139.

Chen Z, Feng J, Saldivar JS, Gu D, Bockholt A, Sommer SS (2008). EGFR somatic doublets in lung cancer are frequent and generally arise from a pair of driver mutations uncommonly seen as singlet mutations: one-third of doublets occur at five pairs of amino acids. *Oncogene* **27**: 4336 4343.

Choong NW, Dietrich S, Seiwert TY, Tretiakova MS, Nallasura V, Davies GC *et al.* (2006). Gefitinib response of erlotinib-refractory lung cancer involving meninges—role of EGFR mutation. *Nat Clin Pract Oncol* **3**: 50 57; quiz 51 p following 57.

Clamp M, Cuff J, Searle SM, Barton GJ. (2004). The Jalview Java alignment editor. *Bioinformatics* **20**: 426 427.

Di Renzo MF, Olivero M, Martone T, Maffe A, Maggiora P, Stefani AD *et al.* (2000). Somatic mutations of the MET oncogene are selected during metastatic spread of human HNSC carcinomas. *Oncogene* **19**: 1547 1555.

Engelman JA, Zejnullahu K, Mitsudomi T, Song Y, Hyland C, Park JO *et al.* (2007). MET amplification leads to gefitinib resistance in lung cancer by activating ERBB3 signaling. *Science* **316**: 1039 1043.

Frohling S, Scholl C, Levine RL, Loriaux M, Boggon TJ, Bernard OA *et al.* (2007). Identification of driver and passenger mutations of FLT3 by high-throughput DNA sequence analysis and functional assessment of candidate alleles. *Cancer Cell* **12**: 501 513.

Guo A, Villen J, Kornhauser J, Lee KA, Stokes MP, Rikova K *et al.* (2008). Signaling networks assembled by oncogenic EGFR and c-Met. *Proc Natl Acad Sci USA* **105**: 692 697.

Hubbard SR. (1997). Crystal structure of the activated insulin receptor tyrosine kinase in complex with peptide substrate and ATP analog. *Embo J* **16**: 5572 5581.

Jackman DM, Holmes AJ, Lindeman N, Wen PY, Kesari S, Borras AM *et al.* (2006). Response and resistance in a non-small-cell lung cancer patient with an epidermal growth factor receptor mutation and leptomeningeal metastases treated with high-dose gefitinib. *J Clin Oncol* **24**: 4517 4520.

Jagadeeswaran R, Ma PC, Seiwert TY, Jagadeeswaran S, Zumba O, Nallasura V *et al.* (2006). Functional analysis of c-Met/hepatocyte growth factor pathway in malignant pleural mesothelioma. *Cancer Res* **66**: 352 361.

Ji H, Ramsey MR, Hayes DN, Fan C, McNamara K, Kozlowski P *et al.* (2007). LKB1 modulates lung cancer differentiation and metastasis. *Nature* **448**: 807 810.

Jin L, Pluskey S, Petrella EC, Cantin SM, Gorga JC, Rynkiewicz MJ *et al.* (2004). The three-dimensional structure of the ZAP-70 kinase domain in complex with staurosporine: implications for the design of selective inhibitors. *J Biol Chem* **279**: 42818 42825.

Jones TA, Zou JY, Cowan SW, Kjeldgaard M. (1991). Improved methods for building protein models in electron density maps and the location of errors in these models. *Acta Crystallogr A* **47**(Part 2): 110 119.

Kobayashi S, Boggon TJ, Dayaram T, Janne PA, Kocher O, Meyerson M *et al.* (2005). EGFR mutation and resistance of non-small-cell lung cancer to gefitinib. *N Engl J Med* **352**: 786 792.

Krause DS, Van Etten RA. (2005). Tyrosine kinases as targets for cancer therapy. *N Engl J Med* **353**: 172 187.

Lo HW, Hsu SC, Ali-Seyed M, Gunduz M, Xia W, Wei Y *et al.* (2005). Nuclear interaction of EGFR and STAT3 in the activation of the iNOS/NO pathway. *Cancer Cell* **7**: 575 589.

Lynch TJ, Bell DW, Sordella R, Gurubhagavatula S, Okimoto RA, Brannigan BW *et al.* (2004). Activating mutations in the epidermal growth factor receptor underlying responsiveness of non-small-cell lung cancer to gefitinib. *N Engl J Med* **350**: 2129 2139.

Ma PC, Jagadeeswaran R, Jagadeesh S, Tretiakova MS, Nallasura V, Fox EA *et al.* (2005a). Functional expression and mutations of c-Met and its therapeutic inhibition with SU11274 and small interfering RNA in non-small cell lung cancer. *Cancer Res* **65**: 1479 1488.

Ma PC, Kijima T, Maulik G, Fox EA, Sattler M, Griffin JD *et al.* (2003a). c-MET mutational analysis in small cell lung cancer: novel juxtamembrane domain mutations regulating cytoskeletal functions. *Cancer Res* **63**: 6272 6281.

Ma PC, Maulik G, Christensen J, Salgia R. (2003b). c-Met: structure, functions and potential for therapeutic inhibition. *Cancer Metastasis Rev* **22**: 309 325.

Ma PC, Schaefer E, Christensen JG, Salgia R. (2005b). A selective small molecule c-MET Inhibitor, PHA665752, cooperates with rapamycin. *Clin Cancer Res* **11**: 2312 2319.

Ma PC, Tretiakova MS, Nallasura V, Jagadeeswaran R, Husain AN, Salgia R. (2007). Downstream signalling and specific inhibition of c-MET/HGF pathway in small cell lung cancer: implications for tumour invasion. *Br J Cancer* **97**: 368 377.

Mazzone M, Comoglio PM. (2006). The Met pathway: master switch and drug target in cancer progression. *FASEB J* **20**: 1611 1621.

Paez JG, Janne PA, Lee JC, Tracy S, Greulich H, Gabriel S *et al.* (2004). EGFR mutations in lung cancer: correlation with clinical response to gefitinib therapy. *Science* **304**: 1497 1500.

Peruzzi B, Bottaro DP. (2006). Targeting the c-Met signaling pathway in cancer. *Clin Cancer Res* **12**: 3657 3660.

Pevarello P, Brasca MG, Amici R, Orsini P, Traquandi G, Corti L *et al.* (2004). 3-Aminopyrazole inhibitors of CDK2/cyclin A as antitumor agents. 1. Lead finding. *J Med Chem* **47**: 3367 3380.

Rikova K, Guo A, Zeng Q, Possemato A, Yu J, Haack H *et al.* (2007). Global survey of phosphotyrosine signaling identifies oncogenic kinases in lung cancer. *Cell* **131**: 1190 1203.

Scapin G, Patel SB, Lisnock J, Becker JW, LoGrasso PV. (2003). The structure of JNK3 in complex with small molecule inhibitors: structural basis for potency and selectivity. *Chem Biol* **10**: 705 712.

Shigematsu H, Gazdar AF. (2006). Somatic mutations of epidermal growth factor receptor signaling pathway in lung cancers. *Int J Cancer* **118**: 257 262.

Shinomiya N, Gao CF, Xie Q, Gustafson M, Waters DJ, Zhang YW *et al.* (2004). RNA interference reveals that ligand-independent met activity is required for tumor cell signaling and survival. *Cancer Res* **64**: 7962 7970.

Smolen GA, Sordella R, Muir B, Mohapatra G, Barmettler A, Archibald H *et al.* (2006). Amplification of MET may identify a subset of cancers with extreme sensitivity to the selective tyrosine kinase inhibitor PHA-665752. *Proc Natl Acad Sci USA* **103**: 2316 2321.

Stamos J, Sliwkowski MX, Eigenbrot C. (2002). Structure of the epidermal growth factor receptor kinase domain alone and in complex with a 4-anilinoquinazoline inhibitor. *J Biol Chem* **277**: 46265 46272.

Tam IY, Chung LP, Suen WS, Wang E, Wong MC, Ho KK *et al.* (2006). Distinct epidermal growth factor receptor and KRAS mutation patterns in non-small cell lung cancer patients with different tobacco exposure and clinicopathologic features. *Clin Cancer Res* **12**: 1647 1653.

Tang Z, Du R, Jiang S, Wu C, Barkauskas DS, Richey J *et al.* (2008). Dual MET-EGFR combinatorial inhibition against T790M-EGFR-mediated erlotinib-resistant lung cancer. *Br J Cancer* **99**: 911 922, 2008.

Thomas RK, Baker AC, Debiasi RM, Winckler W, Laframboise T, Lin WM *et al.* (2007). High-throughput oncogene mutation profiling in human cancer. *Nat Genet* **39**: 347 351.

Wood ER, Truesdale AT, McDonald OB, Yuan D, Hassell A, Dickerson SH *et al.* (2004). A unique structure for epidermal growth factor receptor bound to GW572016 (Lapatinib): relationships among protein conformation, inhibitor off-rate, and receptor activity in tumor cells. *Cancer Res* **64**: 6652 6659.

Zhang X, Gureasko J, Shen K, Cole PA, Kuriyan J. (2006). An allosteric mechanism for activation of the kinase domain of epidermal growth factor receptor. *Cell* **125**: 1137 1149.

Zhu X, Kim JL, Newcomb JR, Rose PE, Stover DR, Toledo LM *et al.* (1999). Structural analysis of the lymphocyte-specific kinase Lck in complex with non-selective and Src family selective kinase inhibitors. *Structure* **7**: 651 661.

Supplementary Information accompanies the paper on the Oncogene website (http://www.nature.com/onc)

Large Cell Neuroendocrine Carcinoma of the Mediastinum with α-Fetoprotein Production

Ken Takezawa, MD, Isamu Okamoto, MD, PhD,* Junya Fukuoka, MD, PhD,† Kaoru Tanaka, MD,* Hiroyasu Kaneda, MD,* Hisao Uejima, MD,‡ Hyung-Eun Yoon, MD, PhD,‡ Masami Imakita, MD, PhD,§ Masahiro Fukuoka, MD, PhD,* and Kazuhiko Nakagawa, MD, PhD**

Large cell neuroendocrine carcinoma (LCNEC) is a relatively new category of pulmonary neuroendocrine tumor. Although it was first detected in the lung, LCNEC has since been found in a variety of extrapulmonary sites. We now describe a patient who was diagnosed with LCNEC originating from the mediastinum, an extremely rare disorder. An increased serum concentration of α-fetoprotein (AFP) in the patient was reduced by chemotherapy in association with tumor shrinkage. Furthermore, the tumor was confirmed immunohistochemically to produce AFP. To our knowledge, this is the first report of a LCNEC that produces AFP.

Key Words: Large cell neuroendocrine carcinoma, α-Fetoprotein, Mediastinal tumor.

(*J Thorac Oncol.* 2008;3: 187–189)

Large cell neuroendocrine carcinoma (LCNEC) is a high-grade neuroendocrine tumor that was first detected in the lung by Travis et al.[1] The prognosis of individuals with LCNEC has been reported to be poor, with a 5-year survival rate similar to that for small cell carcinoma.[2–4] Although originally found in the lung, LCNEC has since been described in a variety of extrapulmonary locations.[5–7] Among these locations, mediastinal LCNEC is extremely rare, with only a few cases having been reported.[8,9] We now report the first case of mediastinal LCNEC with α-fetoprotein (AFP) production.

CASE REPORT

A previously healthy 35-year-old Japanese man was found to have an abnormal mass in his right mediastinum on a chest radiograph during a health checkup. The patient's general condition was fair, and symptoms such as chest pain, weight loss, or fever were not noted. He was a current smoker, having smoked 20 cigarettes a day for 15 years. Computed tomography imaging of the chest revealed a 65 × 50 mm mass in the middle mediastinum (Figure 1*A*). Serum laboratory data were within normal limits. A bronchoscopic examination revealed a compression against the outside of the trachea. No other organs appeared to be affected on extensive examination. Subsequent evaluation for serum tumor markers revealed an increased level of AFP. Other examined markers, including β-human chorionic gonadotropin, carcinoembryonic antigen, and CA19-9, were within normal limits. Thoracoscopic examination revealed that the tumor was not invading into the adjacent lung. On the basis of these findings, we considered the tumor to have originated from the middle mediastinum. A biopsy revealed poorly differentiated carcinoma with neuroendocrine features. Thymic neuroendocrine carcinoma is exclusively located in the anterior-superior mediastinum.[1] Given the tumor's location, the increase in the serum concentration of AFP, and the patient's young age, the diagnosis of embryonal carcinoma was initially favored over purely neuroendocrine neoplasm. The patient received neoadjuvant chemotherapy with bleomycin (30 mg/body) on days 2, 9, and 16, etoposide (100 mg/m^2) on days 1 to 5, and cisplatin (20 mg/m^2) on days 1 to 5. Treatment cycles were repeated every 21 days for 4 cycles. The serum AFP level had decreased to within normal limits in association with shrinkage of the tumor by the end of the third cycle of chemotherapy (Figure 1*B*, *E*). However, the AFP concentration started to increase thereafter, and progression of the tumor was confirmed after the fourth cycle of chemotherapy (Figure 1*C*, *E*). The patient then received second-line chemotherapy with cisplatin (80 mg/m^2) on day 1 and paclitaxel (200 mg/m^2) on day 1 every 21 days for three cycles before surgery. The serum AFP level again decreased in association with tumor shrinkage (Figure 1*D*, *E*). Eight months after initial detection of the tumor, the patient underwent a tumorectomy combined with right upper lobectomy and tracheoplasty, given that the tumor was found to invade the adjacent right upper lobe and trachea at the time of surgery. Histopathologic examination of the surgical specimen revealed a solid tumor nest with massive necrosis. The tumor was relatively homogeneous throughout the resection, showing sheets of cells with a high nucleus-to-cytoplasm ratio. High-power magnification of the tumor revealed that the tumor cells manifested marked neu-

*Department of Medical Oncology, Kinki University School of Medicine, Osaka; †Laboratory of Pathology, Toyama University Hospital, Toyama; ‡Division of Respirology; and §Division of Pathology, Rinku General Medical Center, Osaka, Japan.

Disclosure: The authors declare no conflict of interest.

Address for correspondence: Isamu Okamoto, MD, PhD, Department of Medical Oncology, Kinki University School of Medicine, 377-2 Ohno-higashi, Osaka-Sayama, Osaka 589-8511. E-mail: chi-okamoto@dotd.med.kindai.ac.jp

ISSN: 1556-0864/08/0302-0187

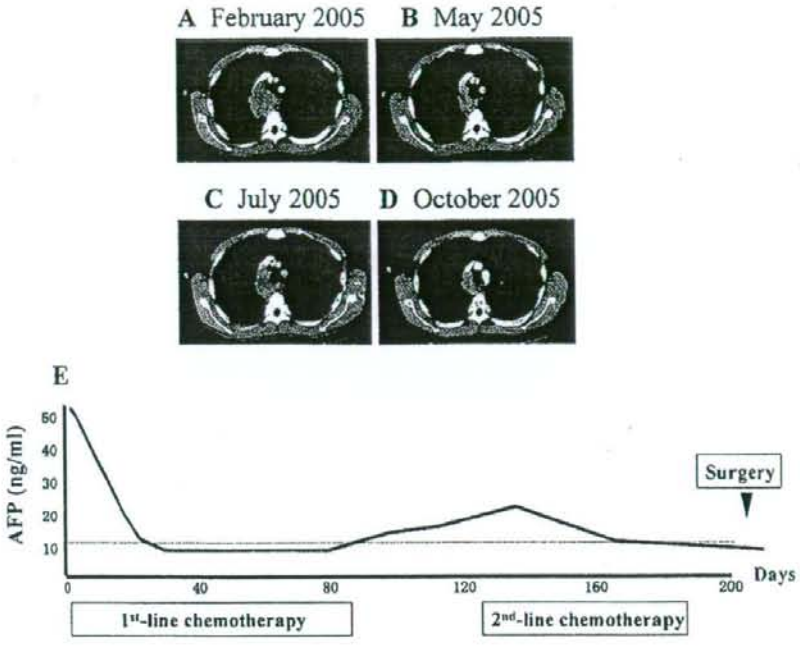

FIGURE 1. Chest computed tomography (CT) findings and serum AFP levels in the patient. *A–D*, Chest CT findings. A mass in the middle mediastinum was initially detected (*A*). The tumor had shrunk after three cycles of neoadjuvant chemotherapy (*B*), but its progression had resumed after the fourth cycle (*C*). The tumor shrank again in response to second-line chemotherapy (*D*). *E*, Time course of the serum concentration of AFP. The AFP level was initially increased, it decreased to within normal limits (dotted line) in association with tumor shrinkage during first-line chemotherapy, but it started to increase again after the third cycle. The serum AFP level again decreased in association with tumor shrinkage during second-line chemotherapy.

roendocrine features, such as frequent rosette structures and trabecular arrangements, nuclear moldings, and prominent mitoses (Figure 2*A*, *B*). The tumor cells also had abundant nucleoli. Immunohistochemical analysis showed the tumor cells to be diffusely positive for CK7 and neuroendocrine markers including CD56, chromogranin A (Figure 2*C*), and synaptophysin as well as negative for CD5, CD30, human chorionic gonadotropin, placental alkaline phosphatase, hepatocyte antigen, and thyroid transcription factor-1. No regions of the specimen showed features of a germ cell tumor or hepatoid carcinoma. On the basis of the morphology and staining characteristics of the tumor, a pathologic diagnosis of LCNEC was made. A small number of tumor cells showed subtle but unequivocal positive staining for AFP (Figure 2*D*). Thoracic radiotherapy was not able to be given because the patient suffered from thoracic empyema after surgery. Despite intensive chemotherapy, he died of extensive recurrence of carcinoma 4 months after the surgery.

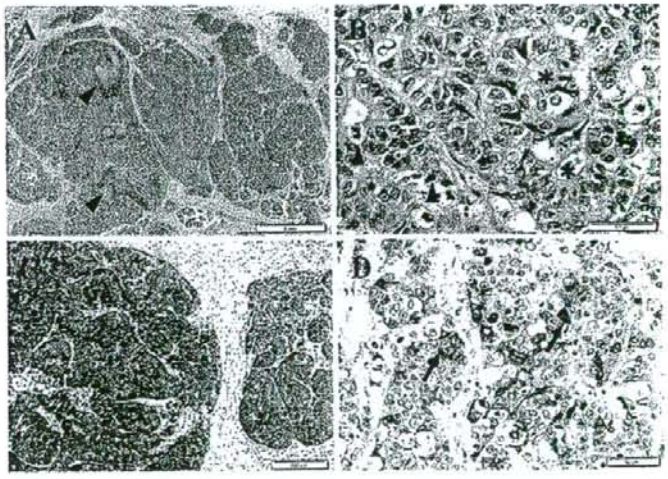

FIGURE 2. Histology and immunohistochemical analysis of the tumor specimen obtained at surgery. *A*, Hematoxylin-eosin staining revealed solid tumor nests with areas of necrosis (arrow heads). Note the homogeneous appearance of the tumor. *B*, High-power magnification of the tumor stained as in (*A*), showing numerous rosettes (asterisk), abundant cytoplasm, chromatin clearing with occasionally prominent nucleoli, nuclear molding (arrows), and frequent mitosis (arrow heads). *C*, Immunohistochemical staining for chromogranin A revealed diffuse and intense cytoplasmic staining. *D*, Immunohistochemical staining for AFP, showing a focus of tumor cells positive for AFP (arrows). Scale bars: 1 mm, 50 μ.

DISCUSSION

LCNEC is a relatively new category of pulmonary neuroendocrine tumor, with affected individuals reported to have a prognosis intermediate between those with atypical carcinoid lung cancer and those with small cell lung cancer.[10] Recent clinical studies indicate a 5-year survival rate of 27 to 67% even if patients are at pathologic stage I.[2–4] Since its original detection in the lung, LCNEC has been found in a variety of extrapulmonary locations including gastrointestinal sites and the uterine cervix.[5–7] The present case was identified as LCNEC originating in the mediastinum. Given the age of the patient and the tumor location, a diagnosis of embryonal carcinoma was initially considered, but no morphologic or immunohistochemical features indicative of embryonal carcinoma were found on extensive pathologic analysis of the surgical specimen. Primary mediastinal LCNEC is an extremely rare disorder and has been described in only a few case reports to date.[8–9]

In the present case, the increased serum AFP level decreased in association with tumor shrinkage in response to chemotherapy, and the tumor was confirmed immunohistochemically to produce AFP. AFP is the main component of fetal serum in mammals. It is synthesized by visceral endoderm of the yolk sac and fetal liver, but expression of the *AFP* gene is greatly reduced at the time of birth. AFP-producing carcinoma has been recognized for decades and reported in various locations including the lung and mediastinum.[11] In contrast to the present case, however, most cancers that produce AFP show morphologic features similar to hepatocellular carcinoma. With regard to neuroendocrine tumors, some case reports indicate that small cell carcinoma can also produce AFP.[12,13] As far as we are aware, however, the present case is the first reported example of LCNEC producing AFP. Given that the concept of LCNEC is relatively new, this may not be that surprising, and previous reports of small cell carcinoma may actually have been diagnosed as LCNEC today. Our case raises the possibility that the origin of mediastinal neuroendocrine tumors including LCNEC may be mediastinal primordial germ cells. Examination of germ cell tumor markers in neuroendocrine tumors may shed light on this matter.

REFERENCES

1. Travis WD, Linnoila RI, Tsokos MG, et al. Neuroendocrine tumors of the lung with proposed criteria for large-cell neuroendocrine carcinoma. An ultrastructural, immunohistochemical, and flow cytometric study of 35 cases. *Am J Surg Pathol* 1991;15:529–553.
2. Iyoda A, Hiroshima K, Toyozaki T, et al. Clinical characterization of pulmonary large cell neuroendocrine carcinoma and large cell carcinoma with neuroendocrine morphology. *Cancer* 2001;91:1992–2000.
3. Takei H, Asamura H, Maeshima A, et al. Large cell neuroendocrine carcinoma of the lung: a clinicopathologic study of eighty-seven cases. *J Thorac Cardiovasc Surg* 2002;124:285–292.
4. Travis WD, Rush W, Flieder DB, et al. Survival analysis of 200 pulmonary neuroendocrine tumors with clarification of criteria for atypical carcinoid and its separation from typical carcinoid. *Am J Surg Pathol* 1998;22:934–944.
5. Jiang SX, Mikami T, Umezawa A, et al. Gastric large cell neuroendocrine carcinomas: a distinct clinicopathologic entity. *Am J Surg Pathol* 2006;30:945–953.
6. Selvakumar E, Vimalraj V, Rajendran S, et al. Large cell neuroendocrine carcinoma of the ampulla of Vater. *Hepatobiliary Pancreat Dis Int* 2006;5:465–467.
7. Tangjitgamol S, Manusirivithaya S, Choomchuay N, et al. Paclitaxel and carboplatin for large cell neuroendocrine carcinoma of the uterine cervix. *J Obstet Gynaecol Res* 2007;33:218–224.
8. Chetty R, Batitang S, Govender D. Large cell neuroendocrine carcinoma of the thymus. *Histopathology* 1997;31:274–276.
9. Nagata Y, Ohno K, Utsumi T, et al. Large cell neuroendocrine thymic carcinoma coexisting within large WHO type AB thymoma. *Jpn J Thorac Cardiovasc Surg* 2006;54:256–259.
10. Moran CA, Suster S. Neuroendocrine carcinomas (carcinoid tumor) of the thymus. A clinicopathologic analysis of 80 cases. *Am J Clin Pathol* 2000;114:100–110.
11. Nasu M, Soma T, Fukushima H, et al. Hepatoid carcinoma of the lung with production of alpha-fetoprotein and abnormal prothrombin: an autopsy case report. *Mod Pathol* 1997;10:1054–1058.
12. Morikawa T, Kobayashi S, Yamadori I, et al. Three cases of extrapulmonary small cell carcinoma occurring in the prostate, stomach, and pancreas. *Indian J Cancer* 1994;31:268–273.
13. Yamaguchi T, Imamura Y, Nakayama K, et al. Paranuclear blue inclusions of small cell carcinoma of the stomach: report of a case with cytologic presentation in peritoneal washings. *Acta Cytol* 2005;49:207–212.

Pharmacokinetic Analysis of Carboplatin and Etoposide in a Small Cell Lung Cancer Patient Undergoing Hemodialysis

Ken Takezawa, MD, Isamu Okamoto, MD, PhD, Masahiro Fukuoka, MD, PhD, and Kazuhiko Nakagawa, MD, PhD

Cancer chemotherapy is not well established for patients on hemodialysis (HD). A 77-year-old man on HD presented with small cell lung cancer. He was treated with the combination of carboplatin and etoposide while the pharmacokinetics of the drugs were monitored. The patient showed a response with manageable toxicity and remained progression free for at least 8 months. The area under the concentration-time curve for each antitumor agent in the patient was within the therapeutic range achieved in individuals with normal renal function. Carboplatin and etoposide chemotherapy combined with HD thus allowed the drugs to achieve an appropriate area under the concentration-time curve and sufficient efficacy in a small cell lung cancer patient with chronic renal failure.

Key Words: Small cell lung cancer, Hemodialysis, Pharmacokinetics, Chemotherapy.

(*J Thorac Oncol.* 2008;3: 1073–1075)

The prognosis of patients with chronic renal failure has improved as a result of progress in hemodialysis (HD), and opportunities to treat malignant tumors that develop in such HD patients are increasing. However, little is known of the safety or efficacy of chemotherapy for malignant tumors in HD patients. We analyzed the pharmacokinetics of combination chemotherapy with carboplatin (CBDCA) and etoposide in a patient with small cell lung cancer (SCLC) undergoing HD.

CASE REPORT

A 77-year-old man with chronic renal failure due to diabetic nephropathy presented with a mass in the left hilar area in March 2007. The general condition of the patient, who had undergone HD, three times a week, was fair, with symptoms such as cough, weight loss, and fever being absent. His Eastern Cooperative Oncology Group performance status was 1. Computed tomography of the chest revealed a 45/33 mm mass in the lower left lobe as well as interstitial pneumonia in the lower left and lower right lobes. Histopathologic analysis of a transbronchial biopsy specimen revealed SCLC. No distant metastasis was detected on systemic examinations, and the patient was diagnosed with limited-stage SCLC. Laboratory testing revealed blood urea nitrogen and creatinine levels of 101 and 8.6 mg/dl, respectively. Other examined laboratory parameters were within normal limits, but subsequent evaluation of serum tumor markers revealed an increased level (18.2 ng/ml) of neuron-specific enolase, which is not affected by renal function.[1]

Radiotherapy was not appropriate for the patient because of his bilateral interstitial pneumonia. Given his good performance status and after obtaining informed consent, we treated the patient with the combination of CBDCA and etoposide (Figure 1). On day 1 of the treatment cycle, the patient received an intravenous injection of etoposide (50 mg/m^2) over 60 minutes followed by an intravenous injection of CBDCA (250–275 mg/m^2) also over 60 minutes. HD was initiated 60 minutes after completion of CBDCA administration and was performed for 4 hours. On day 3, etoposide (50 mg/m^2) was administered over 60 minutes and HD was performed for 4 hours beginning 2 hours after completion of etoposide injection. The doses of CBDCA and etoposide as well as the timing of HD were based on previous studies.[2–4] The treatment was well tolerated. Nonhematologic toxicities such as nausea, vomiting, and fatigue were not observed. The patient also did not experience neutoropenia or thrombocytopenia (Nadir neutrophil and platelet counts during 3 cycles of chemotherapy were 2200/μl and 15.5 $\times$ 10^4/μl, respectively). Prophylactic administration of granulocyte colony-stimulating was not carried out. After three cycles of chemotherapy, each separated by an interval of 3 weeks, the tumor had decreased in size and the serum neuron-specific enolase level had decreased to within normal limits (6.3 ng/ml). The patient remained progression free 8 months after the initiation of treatment.

Pharmacokinetic analysis of CBDCA and etoposide was performed for the first and third courses of chemotherapy. Serial blood samples were collected 0, 1, 2, 3, 4, 5, 6, 24, 37, 41, 42, 49, 53, and 54 hours after completion of CBDCA administration as well as 0, 2, 3, 4, 5, 6, 7, 25, 48, 50, 52, 54, 55, and 73 hours after completion of the first etoposide administration. Each blood sample was analyzed for free

Department of Medical Oncology, Kinki University School of Medicine, Osaka, Japan.

Disclosure: The authors declare no conflicts of interest.

Address for correspondence: Isamu Okamoto, MD, PhD, Department of Medical Oncology, Kinki University School of Medicine, 377-2 Ohno-higashi, Osaka-Sayama, Osaka 589-8511, Japan. E-mail: chi-okamoto@dotd.med.kindai.ac.jp

ISSN: 1556-0864/08/0309-1073

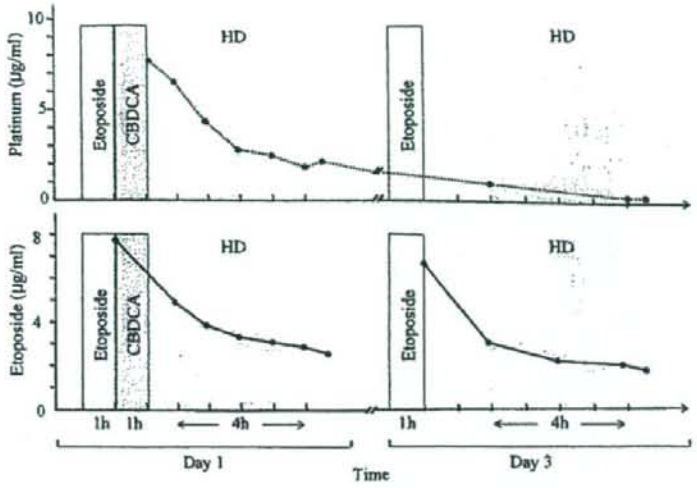

FIGURE 1. Chemotherapy and hemodialysis schedule as well as the plasma concentrations of free platinum and etoposide for the proband. Data are for the first of three cycles of chemotherapy. HD, hemodialysis; CBDCA, carboplatin.

platinum and etoposide (Figure 1) as described previously.[5] In the first cycle, the area under the concentration-time curve (AUC) was 4.10 minutes mg/ml for free platinum and 4401 and 3612 minutes μg/ml for etoposide on days 1 and 3, respectively. In the third course of chemotherapy, for which the CBDCA dose was increased from 250 to 275 mg/m^2, the AUC of free platinum was 4.16 minutes mg/ml. The maximal concentration and half-life of free platinum were 7.7 μg/ml and 2.51 hours in the first cycle and 9.4 μg/ml and 1.93 hours in the third cycle.

DISCUSSION

Many lung cancer patients undergoing HD as a result of impaired renal function may be "undertreated" because chemotherapy regimens are not well established for such individuals. The lack of pharmacokinetic data for most cytotoxic agents in HD patients makes it difficult to administer chemotherapy effectively. Given his old age, bilateral interstitial pneumonia, and renal dysfunction, the present patient might have been considered too high a risk for chemotherapy and recommended to receive best supportive care. However, taking into account the sensitivity of SCLC to platinum combination chemotherapy, we treated him with CBDCA and etoposide while monitoring the pharmacokinetics of these antitumor agents.

CBDCA is a less emetic and less nephrotoxic analog of cisplatin and is preferred over cisplatin for use in patients with renal insufficiency. The desired AUC for CBDCA can be individualized with the use of Calvert's formula on the basis of individual renal function.[6] In previous studies of CBDCA-based chemotherapy in patients undergoing HD, a CBDCA dose of 100 to 150 mg/body was chosen according to this formula, with the glomerular filtration rate set to zero because of the absence of renal function (Table 1).[7–10] In these studies, HD was performed 16 to 24 hours after completion of CBDCA administration, resulting in an AUC of 4.43 to 6.9 minutes mg/ml. More recently, administration of a relatively high dose (300 mg/m^2) of CBDCA with initiation of HD 0.5 to 1.5 hours after completion of drug injection has been shown to be feasible and effective in lung cancer patients undergoing HD.[2–4] However, the AUC of CBDCA in these latter studies was not determined. In the present study, we found that a CBDCA dose of 250 to 275 mg/m^2 administered completely 1 hour before HD gave rise to an AUC for free platinum of 4.10 to 4.16 minutes mg/ml, a therapeutic blood level, consistent with the antitumor efficacy observed

TABLE 1. Previous Studies of Carboplatin-Based Chemotherapy in Cancer Patients on Hemodialysis

	Disease	No. of Patients	Carboplatin Dose	Interval Between Carboplatin Infusion and Hemodialysis (h)	AUC (min mg/ml)
Watanabe et al.[7]	Ovarian cancer	1	125 mg	16	4.43
Jeyabalan et al.[8]	Ovarian cancer	1	125 mg	24	N.D
Chatelut et al.[9]	Ovarian cancer	1	150 mg	24	6.06–6.70
Motzer et al.[10]	Germ cell tumor	2	100 mg/m^2	24	6.7–6.9
Inoue et al.[2]	SCLC	3	300 mg/m^2	1	N.D
Yanagawa et al.[3]	NSCLC/epipharynx ca	2	300 mg/m^2	0.5	N.D
Haraguchi et al.[4]	SCLC	1	300 mg/m^2	1.5	N.D

N.D, not determined; NSCLC, non-small cell lung cancer.